

to those obtained throughout the range 4 to 60 minutes. The fit of the data to the model at 16 minutes is clearly poor; it improves at shorter periods than 16 minutes but deteriorates at longer periods. Over the Coastal Plain, the vertical field amplitudes predicted by the model are too large. Moreover, the model does not predict an appreciable reversal in the real part of the vertical field at periods of 10 minutes and longer despite the generously high conductivities ascribed to the Allegheny Basin (12). We find that the observed attenuation of the vertical fields east of the Blue Ridge requires very high conductivity in the middle to lower crust beneath the Coastal Plain, but this by itself has the unwanted effect on model results of producing large vertical fields, of the wrong sign, west of the Blue Ridge. The observed fields can best be matched by continuing this lower crustal zone, with even higher conductivities, westward under the Appalachians and continental craton.

A two-dimensional conductivity structure which provides a reasonable fit to the data at all periods used is shown in Fig. 2C. This model is not unique, but every model tried that comes close to fitting the data predicts comparable conductivities at similar depths. We could not adequately fit the data with models in which the highly conducting zone was confined to the upper mantle. Besides, high conductivity in the upper mantle is usually associated with high heat flow, high seismic wave attenuation, and low  $P_n$  seismic wave velocities, which are not observed in the region. The proposed conductivity structure—a highly conducting lower crust with a definite lateral variation of conductivity in the vicinity of the Appalachians—is not inconsistent with other geophysical results from this region and elsewhere. High-conductivity lower crustal layers have often been invoked in other areas of the world in the interpretation of geomagnetic variation (9, 13) and magnetotelluric (14) data. The proposed lateral change in conductivity beneath the Blue Ridge coincides with the boundary beneath the eastern and central provinces of the eastern United States defined on the basis of seismic heat flow and gravity data (15). To the east of this boundary the heat flow and Bouguer gravity are higher and the crust is thinner than to the west. Similar lateral variations in conductivity have been reported beneath recent orogenic belts such as the Andes (7) and the Rockies (16) and beneath ancient orogenic zones such as the Canadian Appalachians (4). The former anomalies probably result from unusually high upper mantle temperatures, whereas the latter re-

sult, like our own, is more difficult to explain geochemically or geophysically.

How can the conductivity of crystalline rock at a depth of 15 km be two to three orders of magnitude greater than that at the earth's surface? One explanation is that the rocks of the lower crust in the region are unusually water-rich. An amphibolitic lower crust has already been proposed for the study region (17) on the basis of gravity and seismic refraction data, and it is generally recognized (18) that such hydrated lower crustal rocks could have anomalously high conductivities. It is possible that during subduction at some continental margins segments of oceanic crust become trapped at shallow depths and retain their water-rich character over long periods of time. This would support the idea of Law and Riddihough (19) that conductivity anomalies found today in areas of no obvious tectonism may mark very ancient zones of orogeny and subduction.

R. N. EDWARDS

Department of Physics, University of Toronto, Toronto, Ontario, Canada

J. P. GREENHOUSE

Department of Earth Sciences, University of Waterloo, Waterloo, Ontario 2NL 3G1

#### References and Notes

1. R. J. Banks, *Geophys. J. R. Astron. Soc.* **17**, 457 (1969).
2. D. I. Gough, *Phys. Earth Planet. Interiors* **7**, 379 (1973).
3. An electromagnetic disturbance decays to  $1/e$  of its value measured at the surface of a conductor at a depth  $\delta$  (the skin depth) given by the formula  $\delta = (2/\mu\sigma\omega)^{1/2}$ , where  $\omega$  is the angular frequency,  $\mu$  the magnetic permeability, and  $\sigma$  the conductivity.
4. R. C. Bailey, R. N. Edwards, G. D. Garland, R. D. Kurtz, D. Pitcher, *J. Geomag. Geoelec.* **26**, 125 (1974).
5. W. D. Parkinson, *Geophys. J. R. Astron. Soc.* **2**, 1 (1959).
6. J. E. Everett and R. D. Hyndman, *Phys. Earth Planet Interiors* **1**, 24 (1967).
7. U. Schmucker, S. E. Forbush, O. Hartmann, A. A. Gresecke, Jr., M. Casaverde, J. Castillo, R. Salgueiro, S. del Pozo, *Carnegie Inst. Wash. Yearb.* **66**, 11 (1966/1967).
8. J. P. Greenhouse, R. L. Parker, A. White, *Geophys. J. R. Astron. Soc.* **32**, 325 (1973).
9. R. D. Hyndman and N. A. Cochrane, *ibid.* **25**, 425 (1971).
10. T. R. Madden and C. M. Swift, in *The Earth's Crust and Upper Mantle*, P. J. Hart, Ed. (American Geophysical Union, Washington, D.C., 1969), p. 469.
11. Model resistivities not indicated in Fig. 2 are: seawater, 0.4 ohm-m; upper crustal igneous and metamorphic rocks, 3000 ohm-m; Allegheny Basin sediments, 30 ohm-m; and coastal plain and continental shelf sediments, 20 ohm-m [T. Cantwell, J. W. Galbraith, Jr., P. Nelson, *J. Geophys. Res.* **69**, 4367 (1964)]. Values for the upper mantle were based on Banks's model (1).
12. H. Porath [in *The Structure and Physical Properties of the Earth's Crust*, J. G. Heacock, Ed. (American Geophysical Union, Washington, D.C., 1971), p. 127] has cautioned against the use of two-dimensional models in the vicinity of large sedimentary basins, where current concentrations may be channeled in the sediments from distant regions rather than induced locally. We note, however, that the inland reversed anomaly is not antisymmetric about the deepest part of the Allegheny Basin in Fig. 2, B and C, as would be required for a large current flow in that structure.
13. B. Caner, *J. Geomag. Geoelec.* **22**, 113 (1970).
14. F. L. Dowling, *J. Geophys. Res.* **75**, 2683 (1970).
15. W. H. Diment, T. C. Urban, F. A. Revetta, in *The Nature of the Solid Earth*, F. C. Robertson, Ed. (McGraw-Hill, New York, 1972), p. 544.
16. H. Porath and D. I. Gough, *Geophys. J. R. Astron. Soc.* **22**, 261 (1971).
17. D. E. James, T. J. Smith, J. S. Steinhart, *J. Geophys. Res.* **73**, 1983 (1968).
18. R. D. Hyndman and D. W. Hyndman, *Earth Planet. Sci. Lett.* **4**, 427 (1968).
19. L. K. Law and R. P. Riddihough, *Can. J. Earth Sci.* **8**, 1094 (1971).
20. R. N. Edwards, L. K. Law, A. White, *Philos. Trans. R. Soc. Lond. Ser. A Math. Phys. Sci.* **270**, 289 (1971).
21. U. Schmucker, *Bull. Scripps Inst. Oceanogr. Univ. Calif. No. 13* (1970).
22. J. P. Greenhouse, thesis, University of California, San Diego (1972).
23. We thank the staff of the Fredericksburg Geomagnetic Center for their assistance. The project was funded by the National Research Council of Canada.

16 December 1974

## Aerosols and Polar Temperature Changes

**Abstract.** *Calculations indicate that aerosols are not directly responsible for the present increase in ice abundance in the Northern Hemisphere. Indeed it appears that aerosols cause heating of the atmosphere near the poles. The present background aerosol density at 85°S latitude causes a temperature increase of  $\sim 0.2^\circ\text{K}$ , while that at 85°N causes an increase of  $\sim 0.05^\circ\text{K}$ .*

Kukla and Kukla (1) report that the annual mean snow and ice coverage in the Northern Hemisphere increased by 12 percent in 1971 and that since then the coverage has fluctuated about this higher value. Hamilton and Seliga (2) suggest that aerosol particles in the atmosphere over both polar regions are responsible for the observed changes in surface temperature of the polar ice sheets and hence for ice abundance increases. They assume that aerosols increase the atmospheric turbidity and conclude that this causes a reduction

in the surface temperature. This conclusion is based solely on the globally averaged annual atmospheric calculations of Rasool and Schneider (3). I have investigated the possibility that aerosols over the polar regions are directly responsible for the recent ice and snow increase by calculating, explicitly for summer conditions, the expected temperature change due to aerosols over both 85°N and 85°S latitude.

The physical conditions at both polar regions in summer differ from each other and from the average annual global condi-

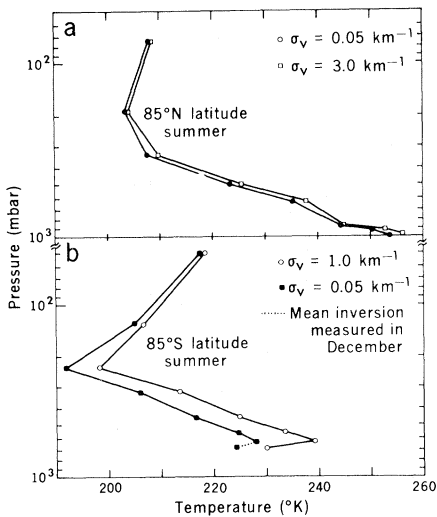


Fig. 1. Calculated asymptotic steady-state temperature as a function of pressure in summer (a) at 85°N, with aerosol particles in the lowest 0.75 km of the atmosphere having  $\sigma_v = 0.05$  and  $3.0 \text{ km}^{-1}$ , and (b) at 85°S, with aerosol particles in the lowest 0.75 km of the atmosphere having  $\sigma_v = 0.05$  and  $1.0 \text{ km}^{-1}$ . The mean inversion measured in December is also shown.

tions in a great many respects, as shown in Table 1. Specifically, near the poles the zenith angle is larger, and the Rayleigh scattering, surface relative humidity, and surface albedo are larger than the global averages. Also, the southern region has a larger surface albedo, elevation, and summer incoming solar radiation flux than the northern region (4).

To define the optical properties of the aerosol particles, I used the approach and parameters of Rasool and Schneider (3) for their mean global calculations. This has been discussed in detail elsewhere (5), and the magnitudes of the parameters are given there. The ratio of the extinction coefficients for visible and infrared radiation is taken to be 0.108, independent of particle number density. The mean visible refractive index is  $1.5 - 0.1i$  (characteristic of Sahara dust) (2).

The physical distribution of  $\text{CO}_2$ ,  $\text{H}_2\text{O}$ , and  $\text{O}_3$  and the physical and optical properties of the water cloud (see Table 2) at 85°N are obtained from experiment 5 of (6). The same parameters (corrected for differences in elevation) are, with the exception of the mean absolute surface humidity, the shortwave albedo, and the cloud cover, used for 85°S. The humidity was determined from mean January relative humidity data collected by Dalrymple (7). The cloud cover was obtained from the averages of observations at three stations (South Pole, Pionerskaya, and Byrd) during January 1957 and five stations (Vostok, Komsomolskaya, South Pole, Pioner-

skaya, and Byrd) during January 1958 (7). To obtain the shortwave surface albedo, the average of midsummer (1957–1958) observations was determined from measurements made on 73 cloudless and 27 overcast days by Hoinkes (8) within 1 km of the South Pole (see Table 2).

All of these factors have been included in a radiative-convective atmospheric model to calculate the role of atmospheric aerosol particles at 85°N and 85°S. The calculation involves forward time integration of the imbalance between solar and terrestrial radiation fluxes calculated at nine different points along the vertical direction, with an appropriate temperature change at each time interval, until an asymptotic approach to a steady-state temperature profile is obtained ( $\leq 0.006^\circ\text{K}$  change in 24 hours).

The principal results are shown in Figs. 1 and 2. Figure 1a shows the calculated asymptotic steady-state temperature profile in the presence of aerosol particles near the surface with visible extinction coefficients,  $\sigma_v$ , of 0.05 and  $3.0 \text{ km}^{-1}$ , at 85°N. Similar curves are shown in Fig. 1b for  $\sigma_v = 0.05$  and  $1.0 \text{ km}^{-1}$  at 85°S. Figure 2 shows the asymptotic steady-state surface temperature at 85°N and 85°S in summer (around July and January) as a function of increasing aerosol  $\sigma_v$  (that is, increasing particle number density). It is evident that the effect of an increase in the number density of aerosol particles is to monotonically increase the temperature of the

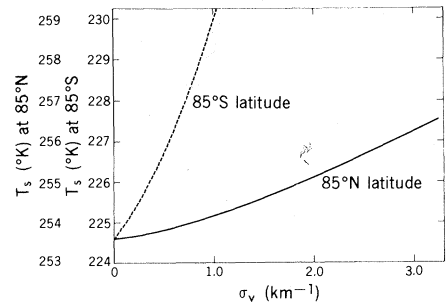


Fig. 2. Calculated values of the mean surface temperature ( $T_s$ ) in summer at 85°N (July) and 85°S (December) as a function of increasing  $\sigma_v$  for aerosol particles located in the lowest 0.75 km of the atmosphere.

polar atmosphere. This result should be compared with the work of Schneider (9), which illustrates that increased cloud cover will decrease the global average temperature but increase the temperature at the poles.

The temperature changes are roughly independent of height in the north polar atmosphere. The vertical temperature distribution for  $\sigma_v = 0.05 \text{ km}^{-1}$  is consistent with the average measured temperature distribution given in a table of supplemental atmospheres of the U.S. Standard Atmosphere, 1962 (10). The temperature changes are larger near the surface in the south polar region. The temperature inversion for  $\sigma_v = 0.05 \text{ km}^{-1}$  is consistent with predictions by Hobbs *et al.* (11), and the mean calculated inversion agrees with

Table 1. Physical conditions at the polar regions in summer compared to annual global average conditions. Abbreviation: ppmv, parts per million by volume.

Property	80°–90°N (July)	80°–90°S (January)	Global average
Time average mean zenith angle, $\cos \theta$	0.318 (14)	0.318 (14)	0.475
Rayleigh scattering	0.08 (6)	0.08 (6)	0.05 (6)
Relative humidity at surface (%)	77 (6)	78 (7)	75 (3)
Shortwave albedo	0.6 (15)	0.89 (7)	0.13 (15)
Surface pressure (mbar)	1000	680 (7)	1000
Mean elevation of surface (m)	137 (15)	2270 (15)	250
Solar radiation at top of atmosphere ( $\text{cal cm}^{-2} \text{ min}^{-1}$ )	1.93 (7)	2.07 (7)	2.00 (15)
$\text{CO}_2$ concentration (ppmv)	320 (3)	320 (3)	320 (3)
Length of daytime (hours)	24	24	12

Table 2. Water cloud properties.

Shortwave		85°N		85°S	
Reflectivity	Absorptivity	Height in atmosphere (mbar)	Cloud cover (%)	Height in atmosphere (mbar)	Cloud cover (%)
0.21	0.005	336	20.5	340.5	34.2
0.48	0.020	664	9.2	452	9.9
0.69	0.035	811–925	37.5	552–630	1.0

the value measured in December by Dalrymple (7). The calculated average daily total radiation ( $\sigma_v = 0.05 \text{ km}^{-1}$ ) reaching the surface at  $85^\circ\text{S}$  is  $\sim 0.62 \text{ cal cm}^{-2} \text{ min}^{-1}$ , compared with a measured value in January over the South Pole of  $0.64 \text{ cal cm}^{-2} \text{ min}^{-1}$  (7). Also, the calculated solar heating rate of the aerosol particles at 630 and 674 mbar is  $\sim 0.96^\circ\text{K}$  per 24-hour day, compared with the value of  $0.5^\circ\text{K}$  per 12-hour day that has been quoted by Hobbs *et al.* (11).

For an assumed present background aerosol  $\sigma_v$  of  $\sim 0.065$  to  $0.1 \text{ km}^{-1}$  (12), the surface temperature change at  $85^\circ\text{N}$  due to these aerosol particles ( $+0.05^\circ\text{K}$ ) is within measured temperature uncertainties. At  $85^\circ\text{S}$  the comparable value is slightly under  $+0.2^\circ\text{K}$ , and averaged over the year this difference would also probably be undetectable.

There is a striking difference between the effect of aerosols over  $85^\circ\text{N}$  and that of aerosols over  $85^\circ\text{S}$ . In the north polar region, a tenfold increase in the background aerosol density would yield a surface temperature rise of  $\sim 0.5^\circ\text{K}$ . In the south a similar increase in particle density would give a rise of  $\sim 5.25^\circ\text{K}$ . Additional calculations have been made to determine the reason for this high sensitivity at  $85^\circ\text{S}$ . It appears that the relative importance of the factors is as follows: thinness of atmosphere  $>$  increased surface albedo  $\gg$  increased solar radiation. Of course the atmospheric system is highly nonlinear and all variations must be considered jointly to obtain the high temperature sensitivity reported here.

I conclude that aerosol particles over the polar regions have not been responsible for the ice mass increase in the Arctic, since they always have a heating effect. Of course, aerosol-induced changes in the general circulation have not been considered here.

Fletcher (13) has indicated that the Southern Hemisphere is the controlling factor in determining the vigor of the global atmospheric circulation. In December both the potential energy and the poleward gradients are equal between the hemispheres, while in June the kinetic energy of the circulation in the south is 3.5 times that in the north. Therefore, an increase of the particle content of south polar atmosphere may have a considerable effect on the air circulation. It may well be that a decrease in the poleward advection (which is not included in these calculations) is responsible for the reduction in the observed polar temperatures.

RUTH A. RECK

Physics Department,  
General Motors Research Laboratories,  
Warren, Michigan 48090

#### References and Notes

- G. J. Kukla and H. J. Kukla, *Science* **183**, 709 (1974).
- W. L. Hamilton and T. A. Seliga, *Nature (Lond.)* **235**, 320 (1972).
- S. I. Rasool and S. H. Schneider, *Science* **173**, 138 (1971).
- M. J. Rubin, *Geophys. Monogr.* **7** (1962), p. 149-159.
- R. A. Reck, *Atmos. Environ.* **9**, 89 (1974); *ibid.* **8**, 823 (1974).
- S. Manabe and R. F. Strickler, *J. Atmos. Sci.* **21**, 361 (1964).
- P. C. Dalrymple, *Am. Geophys. Union Antarct. Res. Ser.* **9**, 195 (1966).
- H. Hoinkes, *Arch. Meteorol. Geophys. Bioklimatol. Ser. B Allg. Biol. Klimatol.* **10**, 175 (1960).
- S. H. Schneider, *J. Atmos. Sci.* **29**, 1413 (1972).
- S. L. Valley, Ed., *Handbook of Geophysics and Space Environments* (McGraw-Hill, New York, 1965), pp. 2-17.
- P. V. Hobbs, H. Harrison, E. Robinson, *Science* **183**, 909 (1974).
- W. M. Porch, R. J. Charlson, L. F. Radke, *ibid.* **170**, 315 (1970).
- J. O. Fletcher, *The Polar Oceans and World Climate* (P-3801, Rand Corporation, Santa Monica, Calif., 1968); *Changing Climate* (P-3933, Rand Corporation, Santa Monica, Calif., 1968).
- S. Manabe and F. Möller, *Mon. Weather Rev.* **89**, 503 (1961).
- W. D. Sellers, *Physical Climatology* (Univ. of Chicago Press, Chicago, 1969).
- I thank R. T. Wetherald and S. Manabe of the Geophysical Fluid Dynamics Laboratory/NOAA at Princeton University for a copy of their radiative-convective atmospheric code into which I introduced the role of aerosol particles.

2 October 1974; revised 9 December 1974

## Uniflagellate Spermatozoa in Nemertoderma (Turbellaria) and Their Phylogenetic Significance

Abstract. *An ultrastructural study of Nemertoderma (Turbellaria, Nemertodermatida) has revealed that its spermatozoa have only a single flagellum. This is the first uniflagellate spermatozoon known in the Turbellaria; it is indicative of the primitiveness of Nemertoderma and is evidence in support of the view that the Turbellaria as a whole are among the most primitive living Bilateria.*

Many theories on the origin and evolution of the Metazoa consider the Turbellaria to be the most primitive of all Bilateria (1). The finding in recent years, however, that all Platyhelminthes, including the Turbellaria, have biflagellate, or occasionally aflagellate, spermatozoa (2), has been a serious obstacle to the acceptance of these theories. Since the occurrence in most metazoan phyla of uniflagellate sperm indicates that the primitive spermatozoon type was uniflagellate (3), the turbellarians, with their biflagellate spermatozoa, seem to be well removed from the metazoan ancestor. We have found, however, that the spermatozoa of *Nemertoderma*, a primitive marine turbellarian (4, 5), are uniflagellate and sufficiently similar to the hypothetical primitive spermatozoon to establish the Turbellaria again near the base of the phylogenetic tree of the Bilateria.

Specimens of an undescribed species of *Nemertoderma* [*Nemertoderma* sp. A (6)] from the shallow subtidal off Bogue Bank, N.C., were fixed in phosphate-buffered 2.5 percent glutaraldehyde plus 2 percent tannic acid, postfixed in phosphate-buffered 2 percent  $\text{OsO}_4$ , and embedded in a mixture of Epon and Araldite. Thin sections from the embedment blocks were stained with uranyl acetate and lead citrate and examined with a Zeiss electron microscope.

The spermatozoa in *Nemertoderma* sp. A are grouped in bundles in the testis. In transverse sections of these bundles (Figs. 1 to 3), the spermatozoa can be seen to have three easily distinguished regions: a head, with the nucleus; a middle piece, with what are presumed to be mitochondrial de-

rivatives partially enwrapping the single flagellar axoneme; and a tail, with the continuation of the flagellar axoneme. The spermatozoa are uniflagellate and the axoneme of the flagellum has a regular  $9 + 2$  pattern of microtubules. No centriole, in the sense of a  $9 + 0$  triplet microtubule structure, is to be seen in the mature sperm. Instead, the  $9 + 2$  axoneme inserts directly into a small fossa in the posterior end of the nucleus, and the central pair of singlets is continuous all the way into the base of this fossa. The only character that differentiates this basal part from the rest of the axoneme is the presence of a set of  $0.3\text{-}\mu\text{m}$ -long peripheral dense fibers contiguous with the outer edge of each doublet (Figs. 2 and 4).

The axoneme is the only organelle to be seen through most of the sperm tail; it is not present, however, in the extreme tail tip where instead numerous loosely packed singlet microtubules are seen (Fig. 3).

The nucleus of the mature spermatozoon is a highly condensed structure approximately  $6.5 \mu\text{m}$  long and  $0.25 \mu\text{m}$  wide, with a deep longitudinal spiral groove (Fig. 1). At its tip is a simple vesicle,  $0.3 \mu\text{m}$  long, evidently an acrosome. Such an organelle has not been identified in any other turbellarian spermatozoa (7).

The middle piece of the spermatozoon (Figs. 2 and 4) is as long as the nucleus ( $6.5 \mu\text{m}$ ). Its cytoplasm is homogeneous and finely granular. A row of six to eight dense crescent-shaped bodies embedded in this cytoplasm, each with one, two, or occasionally three vesicular structures, are presumably mitochondrial derivatives.

According to Franzén (3), who has con-